PROCEEDINGS OF SCIENCE

Search for ultra-High Energy Photons with the Pierre Auger Observatory

Mariangela Settimo[*1] **for the Pierre Auger Collaboration**[2]

[1] *LPNHE, Paris VI-VII, 4 Place Jussieu, 75252 Paris cedex 05, France*
[2] *Observatorio Pierre Auger, Av. San Martín Norte 304, 5613 Malargüe, Argentina*
(Full author list: http://www.auger.org/archive/authors_2013_05.html)
E-mail: mariangela.settimo@lpnhe.in2p3.fr

The Pierre Auger Observatory, located near Malargüe, in the Province of Mendoza, Argentina, was designed and optimized to investigate the origin and the nature of ultra-high energy (UHE) cosmic rays, above 10^{18} eV, using a hybrid detection technique. Its large collection area coupled with the information from the surface array of water Cherenkov detectors and from the fluorescence telescopes, provide a unique opportunity to search for UHE photons. Current results and the latest upper limits on the diffuse flux of photons are presented.

International Conference on the Structure and the Interactions of the Photon including the 20th International Workshop on Photon-Photon Collisions and the International Workshop on High Energy Photon Linear Colliders
20 - 24 May 2013
Paris, France

[*]Speaker.

PoS(Photon 2013)062

1. Introduction

Ultra-high energy photons, with energy higher than 10^{18} eV, are one of the theoretically plausible candidates to be part of the flux of UHE cosmic rays. A fraction of photons, typically (0.01-1)% of the all-particle flux above 10^{19} eV, is expected as a by-product of the photo-production of pions by cosmic rays interacting with the microwave background (the so called Greisen-Zatsepin-Kuz'min or GZK effect [1, 2]). The existence of such a process can be tested by the observation of a cut-off of the all-particle energy spectrum above about $10^{19.5}$ eV. Such a suppression of the cosmic-ray flux has been observed, with high significance, by the Pierre Auger Observatory [3, 4] and independently by the Telescope Array and HiRes experiments [5, 6]. However, other scenarios, such as a limitation in the maximum acceleration power of the astrophysical sources, could conceivably produce a similar spectral feature and cannot be excluded with the current results. The observation of a photon component would be an independent probe of the origin of this flux suppression and could possibly prove the GZK effect. A large fraction ($\sim$ 50%) of photons in the cosmic-ray spectrum is also predicted within most "top-down" models (e.g., super-heavy dark matter, Z-burst, topological defects) which had been introduced to explain the origin of cosmic rays at the highest energies [7]. Constraints on these models can be imposed by the observation (or non-observation) of UHE photons.

Given their extremely low flux, UHE photons (and cosmic rays) can be detected only by means of the extensive air showers (EAS) induced when the primary particle enters the atmosphere. The development of these cascades of secondary particles, as well as the types and the abundances of secondaries, are related to the chemical nature and the energy of the primary particle. The identification of UHE photons relies on the accurate determination of the shower's features and on the fact that EAS initiated by primary photons have different developments and a different content of secondary particles. The Pierre Auger Observatory [8], with its hybrid concept and its huge exposure, allow us to perform a search for UHE photons with unprecedented statistics and by using independent, complementary techniques. In this proceeding the search for a diffuse photon flux, performed at the Auger Observatory, is reviewed and a brief description of the phenomenology of EAS induced by photons is also provided by way of introduction.
A directional search for photons, complementing the results given here, has also been carried out and is discussed in detail in [9].

2. Photon identification

One of the most robust and powerful observables for the discrimination of photons and for mass composition studies is $X_{\rm max}$, which is defined as the atmospheric depth at which a shower reaches its maximum development (in terms of particle count or energy deposit). In particular, air showers induced by photons are expected to develop deeper in the atmosphere (i.e., resulting in a larger value of $X_{\rm max}$) because of the smaller average multiplicity in electromagnetic interactions as compared to hadronic ones. The average $X_{\rm max}$ for photon and nuclear primary cosmic rays is shown in Fig. 1 as a function of energy. Given the lack of detailed knowledge on the hadronic interactions at ultra-high energies, different model predictions [11, 12, 13], updated according to the most recent LHC results, are also given for nuclei. Contrariwise, photon simulations only rely on the

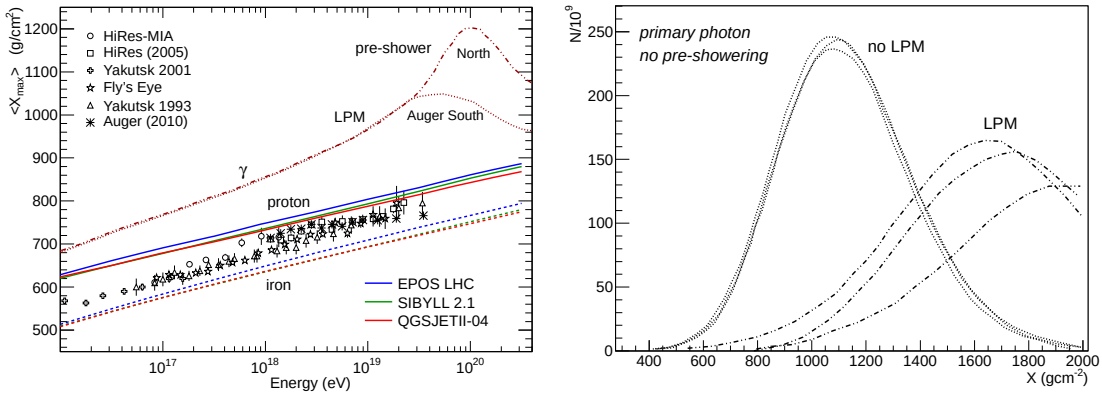

Figure 1: Left: Average $X_{\max}$ of photon and nuclear cosmic ray primaries, as a function of energy. Different hadronic interaction models are plotted for nuclear primaries [10]. Right: Particle count as three sample showers develop, as a function of atmospheric depth, illustrating the impact of the Landau-Pomeranchuk-Migdal effect on the longitudinal development of photon induced showers [16].

well-known electromagnetic processes, making more robust the predictions of the features of the EAS. As shown in Fig. 1, the $X_{\max}$ for photon showers is typically a few hundred g/cm^2 larger than nuclei with the same energy. Moreover, as a consequence of the deeper development and a much reduced abundance of muons, photon showers are expected to have a smaller size at the ground, a steeper lateral distribution of secondary particles, a sparser distribution of arrival times of particles in the shower front and a larger delay with respect to a planar shower front approximation. The differences between photons and nuclear primaries are further enhanced at energies above 10^{19} eV because of the Landau-Pomeranchuk-Migdal (LPM) effect [14, 15] which suppresses the cross-section for a symmetric electron pair production. Because of this effect, the development of the air shower is slowed and the event by event fluctuations are enhanced (see Fig. 1, right) [16, 17].

At higher energies, above 50 EeV (1 EeV = 10^{18} eV), photons entering the atmosphere have a non-negligible probability to convert in the geomagnetic field, producing e^+/e^- pairs which then emit synchrotron photons. The probability of photon conversion and of synchrotron emission by the electrons (or positrons) depends on the energy of the photon and on the component of the local magnetic field orthogonal to the direction of the particle's motion [18, 19]. For converted photons, a bunch of low-energy electromagnetic particles, called a "preshower", is thus entering the atmosphere. Nevertheless, since the spread of the preshower particles in transverse distance and in arrival time is well below the detector resolutions, the air shower is observed as one single event. The impact of the preshower on the average $X_{\max}$ is shown in Fig. 1 (left) at the Auger South site: because of the local magnetic field, the preshowering effect is stronger for photons arriving from the south direction than from the north. In addition, converted showers are expected to have a flatter lateral distribution and smaller fluctuations than unconverted photons. In Fig. 2, the impact of the preshowering on the longitudinal profile and on the number of muons is shown assuming two different site locations (i.e., two different conversion probabilities). Whereas significant differences are observed for the average value and the spread of $X_{\max}$ for converted and unconverted photons, the number of muons remains significantly smaller for photons than for nuclei, and the differences

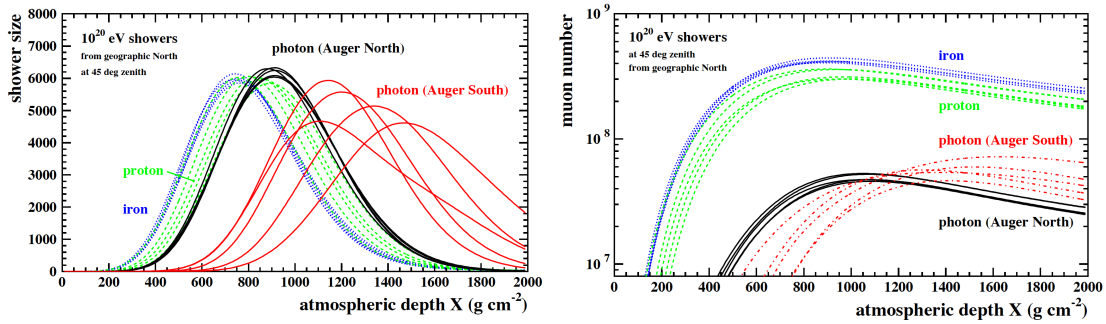

Figure 2: Impact of the preshowering effect on the longitudinal development of a shower (left) and on the evolution of the muon population with atmospheric depth (right) [20].

between the converted and unconverted cases are in part due to the different $X_{\max}$.

3. The Pierre Auger Observatory

The Pierre Auger Observatory, located near Malargüe (province of Mendoza, Argentina) consists of an array of over 1600 water Cherenkov Surface Detectors (SD) [21] deployed over a triangular grid of 1.5 km spacing and covering an area of 3000 km^2. The ground array is overlooked by 27 fluorescence telescopes, grouped in five sites, making up the fluorescence detector (FD) [22]. Whereas the SD samples the density of secondaries at the ground, the FD observes the longitudinal development of the shower in the atmosphere (i.e., the energy deposit as a function of the atmospheric depth) by detecting the fluorescence light emitted by excited nitrogen molecules and the Cherenkov light induced by shower particles in air. Using FD, the electromagnetic energy released by the shower in the atmosphere can be measured from the integral of the longitudinal profile and the total energy of the primary particle is then derived by correcting for the invisible energy carried by penetrating particles. Thus the FD provides a calorimetric measurement of the primary energy, in a way that is only weakly dependent on the primary type and on the details of the hadronic interaction models. However, unlike the SD array, the FD may only operate during clear and moonless nights and thus with a duty cycle reduced to about 13% [23]. Since the fluorescence emission and the light scattering and attenuation depend on atmospheric conditions, several systems monitor the weather conditions, the aerosol content and the cloud coverage over the array [24]. Events detected by at least one FD telescope and one SD station are named “hybrids”. For these events, the combination of the timing information from the FD and the SD provides an accurate determination of the geometry of the air showers. The hybrid events allow a calibration of the SD energy estimator (i.e., the signal recorded at 1000 m from the shower axis), reducing the dependence on hadronic models generally associated with SD-based measurements. Moreover, in hybrid mode, the complementary SD and FD mass sensitive parameters can be used together to improve the photon identification.

3.1 Photon search with SD

The photon search with SD has been conducted using the shower front radius of curvature (R) and the signal risetime at 1000 m from the shower axis ($t_{1/2}(1000)$), as these two observables are connected to shower development and muon content [25]. In fact, due to geometrical reasons, the

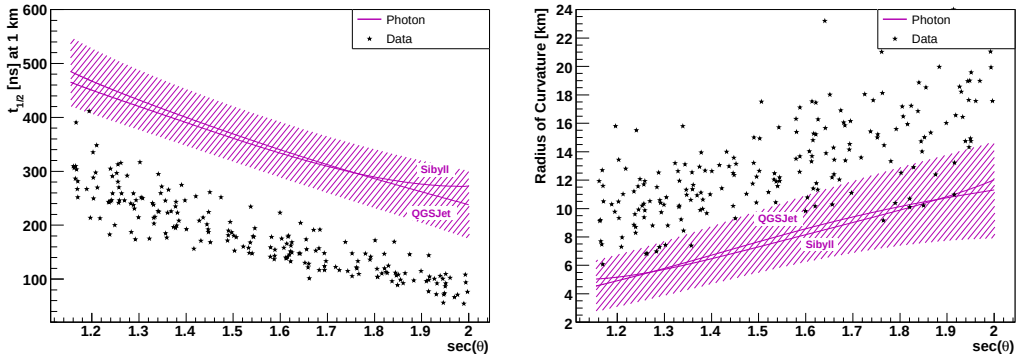

Figure 3: Risetime $t_{1/2}$ and radius of curvature R for SD events as a function of $\sec(\theta)$. The shaded area indicates the expectation for photons while points are the data collected from 2004 up to 2006 [25].

shower front can be represented, to a first approximation, by a sphere with a radius of curvature R that depends on the $X_{\max}$. Events developing deeper in atmosphere (i.e., photon-like) are expected to have smaller radius R than nuclei. Moreover, showers with a larger muon content have typically a larger radius of curvature since the muons reaching the ground are generally produced at higher altitudes and they have a smaller time spread than the electromagnetic component. Concerning the second observable, for each SD station the risetime $t_{1/2}$ is defined as the time to increase from 10% to 50% of the total signal deposited in that station. The risetime at 1000 m, $t_{1/2}(1000)$, is then derived from a fit of the risetime in each station with a quadratic function of distance. In Fig. 3 the signal risetime (left panel) and the radius of curvature of the shower front (right panel) are shown as a function of $\sec(\theta)$, with θ the zenith angle of the incident parent, for a subset of the data and for photon simulations. Data points, which are expected to be dominated by nuclear primaries, are distributed differently from photon expectations. The separation power of the risetime and the radius of curvature is strengthened by a combination of these two observables through a principal component analysis (PCA). The training of the PCA is performed using photon simulations and 5% of the acquired data (see Fig. 4, left). Such a choice is due to the lack of knowledge of the hadronic interaction models, and consequently on the prediction of the particle distribution at the ground, which is especially important for SD observables. It is worth remarking that, for SD, the energy estimator is the signal at 1000 m, $S(1000)$, which is related to the size of the shower at the ground, and consequently to the energy of the primary particle. However, for photon and hadron primaries with the same initial energy, the expected value of S(1000) may be a factor 2 smaller, because of the lower muonic content in photon showers. For this reason two different energy scales have been used in the analysis. The one for nuclear primaries is obtained by calibrating the collected data with the energy measured by FD [26], while the energy scale for photons is derived using the measured S(1000) and the expectation from photon simulations. The procedure is described in detail in [27].

The search for photons has been carried out for the data recorded by the surface detector between January 2004 and December 2006 [25]. Given the steep lateral distribution of photon primaries and their smaller muon content, the SD array is fully efficient to photon events at energies higher than for nuclei, and the analysis here is thus limited to events with energies above 10^{19} eV and with zenith angles between 30° and 60°. For a reliable determination of the risetime and of the

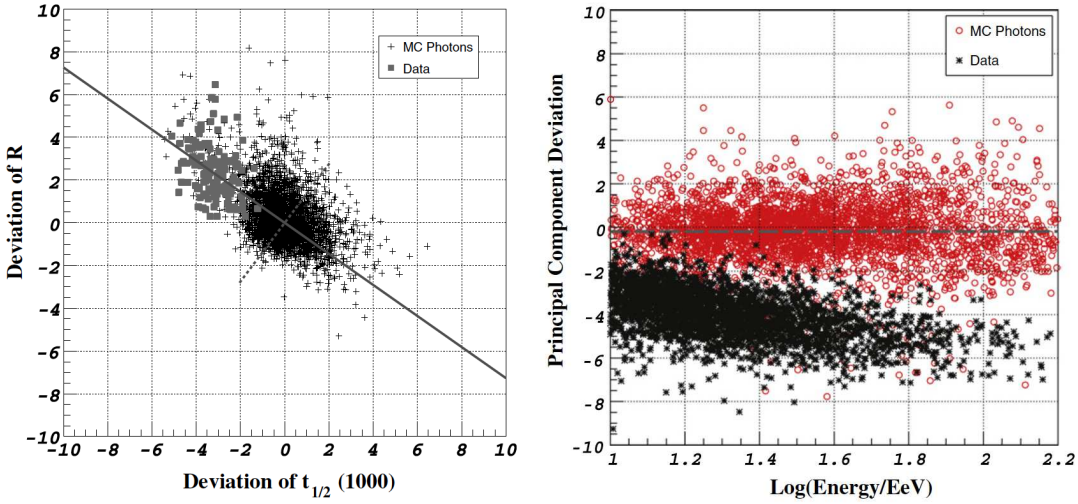

Figure 4: Left: Deviations of R and $t_{1/2}(1000)$ from photon predictions for 5% of the data (squares) and for photon simulated events (black pluses). The solid line is the principal component axis. Right: PCA response for data (black asteriscs) and photons (red open circles) as a function of the primary photon energy. In both figures, the dashed line indicates the cut at the median of the photon distribution (see text) [25].

radius of curvature, only events are selected which are well contained in the array, and which have at least 5 stations each with a signal larger than 10 VEM (vertical equivalent muon), before applying the principal component analysis. Once the PCA is trained and applied to data, photon-like events are selected with an "a priori" cut set at the median of the distribution of the PCA variable of the simulated photon sample (Fig. 4, right). No photon-like events were found, and upper limits to the integral photon flux are obtained for three different energy thresholds E_0 = 10, 20, 40 EeV:

$$\phi_\gamma^{95CL} = \frac{N_\gamma^{95CL}(E_\gamma > E_0)}{0.95A \times f \times \varepsilon}. \tag{3.1}$$

where A is the geometrical aperture of the SD array, 0.95 is the fraction of data used for the analysis, f and $\varepsilon = 0.5$ are the efficiencies of the selection of good events and of the PCA "a-priori" cut, respectively. The limits obtained from this analysis are discussed in section 4.

3.2 Photon search with Hybrids

At energies less than 10^{19} eV, the photon search has been performed by taking advantage of the low energy threshold and the high quality of events detected in hybrid mode [28, 29]. Since the FD provide a direct measurement of the longitudinal profile, the analysis benefits from the direct observation of the $X_{\rm max}$. Moreover, to improve the photon-hadron discrimination power we complement the $X_{\rm max}$ with an SD observable, S_b, defined in [30] as

$$S_b = \sum_i S_i \left(\frac{R_i}{R_{\rm ref}}\right)^b \tag{3.2}$$

where the sum runs over the triggered stations, S_i is the recorded signal in the station at distance R_i from the hybrid reconstructed axis and $R_{\rm ref}$ is a reference distance equal to 1000 m for this analysis.

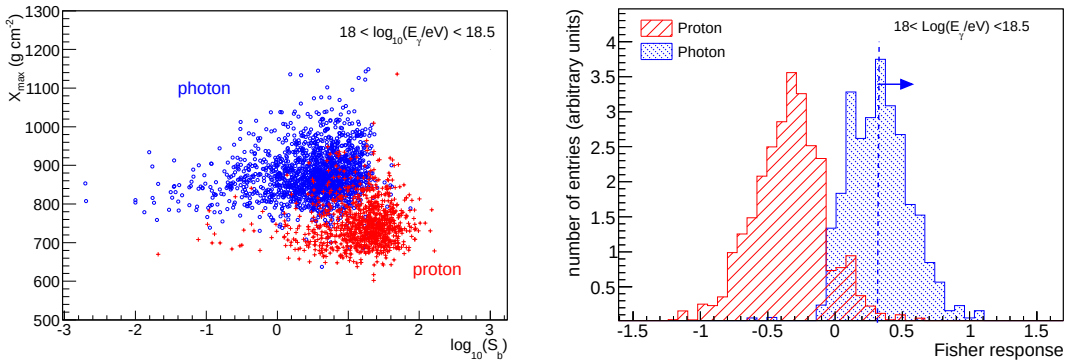

Figure 5: Left: Simulated distribution of $X_{\rm max}$ as a function of $\log_{10}(S_b)$ for proton (red crosses) and photon (empty blue circles) showers with energy between 10^{18} and $10^{18.5}$ eV. Right: Distribution of the Fisher response parameter for proton (red) and photon (blue) for simulated showers with energy between 10^{18} and $10^{18.5}$ eV. Photon-like events are selected requiring a Fisher value larger than X_{cut} (dashed line) as indicated by the arrow.

The exponent b is chosen equal to 4 which maximizes the separation power between photons and hadrons in this energy range. The S_b parameter combines the varying strength of the signal in the surface detector and the steeper lateral distribution function expected for photon-induced showers. Events with zenith angle less than 60° and with a good geometric reconstruction are selected for the analysis. Moreover, to ensure an accurate $X_{\rm max}$ measurement, we require a good fit of the longitudinal profile to a Gaisser-Hillas function, an $X_{\rm max}$ that is observed within the field of view of the FD telescopes, a Cherenkov light contamination smaller than 50% and an uncertainty on the reconstructed energy of at most about 20%. To reject misreconstructed profiles, only time periods with the sky not obscured by clouds and with a reliable measurement of the vertical aerosol optical depth are selected. On the SD side, at least 4 active stations are required to be within 2 km from the hybrid reconstructed axis. This prevents any underestimation of S_b (which would mimic the behavior of a photon event) due to missing (not deployed or temporarily inefficient) detectors.

To carefully reproduce the operating conditions of the data acquisition, time-dependent simulations are performed according to the hybrid detector on-time history [23], also taking into account the actual atmospheric conditions. The correlation between $X_{\rm max}$ and S_b is shown in Fig. 5 (left) for photon (empty blue circles) and proton (red crosses) showers, in the energy interval between 10^{18} and $10^{18.5}$ eV. Photon-like events are expected to lie in the top-left part of the distribution because of the deeper $X_{\rm max}$ and of the smaller S_b. For the classification of photon candidates, and to enhance the discrimination capabilities of $X_{\rm max}$ and S_b, the two observables are combined in a Fisher analysis trained on a sample of photon and proton showers. The Fisher response parameter distribution is shown in Fig. 5 (right) for photon and proton primaries. Similarly to the SD-alone analysis, photon-like events are selected by applying an "a priori" cut at the median of the distribution of the Fisher response for photons. This approach provides a conservative upper limit by reducing the dependence on the hadronic interaction models and on the mass composition assumption. With this choice the expected hadron contamination is about 1% in the lowest energy interval (between 10^{18} eV and $10^{18.5}$ eV) and it becomes smaller for increasing energies.

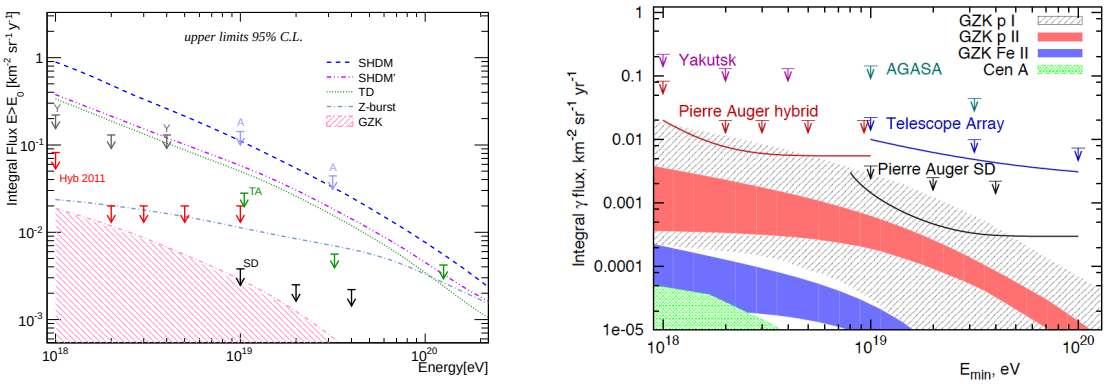

Figure 6: Left: Upper limits on the integral photon flux derived by Auger with the hybrid [28] and SD [25] detectors, compared to the results of AGASA (A) [32] and Yakutsk (Y) [33]. The shaded region and the lines give the predictions for the GZK photon flux and for top-down models, respectively (TD, Z-Burst, SHDM from [7] and SHDM' from [34]). Right: the same plot but including also the estimates of the sensitivity with data until 2015, as derived by scaling the current limits to account for the relative expected increase of the exposure, and assuming that the number of background events remains constant. The shaded regions are the predictions from [7] assuming protons at the source (gray band), from [35] (red and blue, under the assumption of proton and iron acceleration), and for the case of a single source as Centaurus A [36] (green).

Applying the method described above to the data collected between January 2005 and September 2010, we found 6, 0, 0, 0 and 0 photon candidates for energies above 1, 2, 3, 5 and 10 EeV, respectively. We checked with simulations that the observed number of photon candidates is consistent with the expectation from nuclear primaries, within the assumption of a mixed composition. In addition, for each of the photon candidates, the background contamination was individually checked by simulating 1000 dedicated CORSIKA proton showers with the same energy, arrival direction and core position as reconstructed for the real events. The actual SD and FD configurations at the detection time are also considered. For each of the analysed candidates we found that a fraction of proton induced showers between 1% and 2% can be wrongly selected as photon-like events.

Given this result, upper limits (ϕ_γ^{95CL}) have been obtained at the 95% confidence level on the photon flux integrated above an energy threshold E_0:

$$\phi_\gamma^{95CL} = \frac{N_\gamma^{95CL}(E_\gamma > E_0)}{\mathcal{E}_{\gamma,\mathrm{min}}}. \tag{3.3}$$

where E_γ is the reconstructed energy assuming that the primary particle is a photon (i.e., the calorimetric energy measured by FD plus a correction of about 1% due to the invisible energy [31]), N_γ^{95CL} is the number of photon candidates above E_0 at the 95% confidence level and $\mathcal{E}_{\gamma,\mathrm{min}}$ is the exposure of the hybrid detector [3]. To be conservative, the minimum value of the exposure above E_0 is used in equation (3.3) and a possible nuclear background is not subtracted for the calculation of N_γ^{95CL}.

4. Discussion and Outlook

No photon events have been identified so far with either the SD or the hybrid analysis. Upper

bounds on the integral photon flux have been placed and are shown in Fig. 6. From hybrid analysis, upper limits of 8.2×10^{-2} km^{-2} sr^{-1} y^{-1} above 1 EeV and 2.0×10^{-2} km^{-2} sr^{-1} y^{-1} above 2, 3, 5 and 10 EeV have been derived (red arrows). At higher energies, limits of 3.8×10^{-3}, 2.5×10^{-3}, 2.2×10^{-3} km^{-2} sr^{-1} y^{-1} are obtained from the SD analysis (black arrows). Other experimental results (AGASA [32] and Yakutsk [33]) and model predictions [7, 34] are also shown for comparison. The derived bounds correspond to a fraction of photons of about 0.4%, 0.5%, 1.0%, 2.6% and 8.9% for energies above 1, 2, 3, 5 and 10 EeV, respectively and to 2.0%, 5.1%, 31% above 10, 20 and 40 EeV, respectively. The robustness of these results was checked against hadronic interaction models and chemical composition, as well as the resolutions in the measurement of the discriminating observables and the energy determination. We refer to the papers [25] and [28] for detailed discussions. The current results of the Auger Observatory disfavor the exotic models for the origin of UHECR available in [7, 34] over a wide energy range, and the region of the expected GZK photon flux in the most optimistic scenarios will be within reach in the next few years. An estimate of the sensitivity to photon fluxes with data collected until 2015 is illustrated in the left panel of Fig. 6. It is derived by scaling the current limits to account for the relative expected increase of the exposure, and assuming that the number of background events remains constant. Such results may have a potential impact to understand the cut-off at the end of the energy spectrum, to prove (or disprove) the existence of the GZK process and to constrain astrophysical and top-down scenarios for the origin of UHECRs. Moreover, the observation (or non-observation) of UHE photons can have implications on fundamental physics since the predicted flux of GZK photons can be affected by any Lorentz Invariance Violation (see for example [37]) or by possible photon-axion conversion [38] during photon propagation.

References

[1] K. Greisen, Phys. Rev. Lett., 1966 **16**:748.

[2] G.T. Zatsepin, V.A. Kuz'min, Pis'ma Zh. Eksp. Teor. Fiz., 1966, **4**(3): 114.

[3] M. Settimo, for the Pierre Auger Collaboration, Eur. Phys. J. Plus, 2012, **127**: 87.

[4] A. Schultz, for the Pierre Auger Collaboration, Proc. 33rd Int. Cosmic Ray Conf. (ICRC 2013), arXiv:1307.5059.

[5] R. Abbasi *et al.*, HiRes Collaboration, Phys. Rev. Lett., 2008, **100**: 101101.

[6] Telescope Array Collaboration, submitted to PRL, arXiv:1205.5067v1.

[7] G. Gelmini, O. Kalashev, D. Semikoz, J. Exp. Theor. Phys., 2008, **106**: 1061.

[8] The Pierre Auger Collaboration, Nucl. Instrum. Meth. A, 2004, **523**(1): 50.

[9] D. Kuempel, for the Pierre Auger Collaboration, Proc. 33rd Int. Cosmic Ray Conf. (ICRC 2013), arXiv:1307.5059.

[10] D. Heck *et al.,"CORSIKA: A Monte Carlo Code to Simulate Extensive Air Showers"*, Report FZKA, 1998, **6019**.

[11] S. Ostapchenko, Phys. Rev. D, 2011, **83**: 014018.

[12] K. Werner, I. Karpenko, and T. Pierog, Phys. Rev. Lett., 2011, **106**: 122004

[13] E.J. Ahn, R. Engel, T.K. Gaisser, P. Lipari, T. Stanev, Phys. Rev. D, 2009, **80**: 094003.

[14] L.D. Landau, I.Ya. Pomeranchuk, Dokl. Akad. Nauk, SSSR, 1953, **92**: 535.

[15] A.B. Migdal, Phys. Rev., 1956, **103**: 1811.

[16] M. Risse, P. Homola, Mod. Phys. Lett. A, 2007, **22**: 749, astro-ph/0702632.

[17] X. Bertou, P. Billoir, S. Dagoret-Campagne, Astropart. Phys., 2000, **14**.

[18] T. Erber, Rev. Mod. Phys., 1966, **38**: 626.

[19] B. McBreen and C.J. Lambert, Phys. Rev. D, 1981, **24**, 2536.

[20] P. Homola et al., Astropart. Phys., 2007, **27**: 174, astro-ph/0608101.

[21] The Pierre Auger Collaboration, Nucl. Instrum. Meth. A, 2010, **613**(1): 29.

[22] The Pierre Auger Collaboration, Nucl. Instrum. Meth. A, 2010, **620**(2): 227.

[23] The Pierre Auger Collaboration, Astropart. Phys., 2011, **34**: 368.

[24] L. Valore for the Pierre Auger Collaboration, Proc. 31st Int. Cosmic Ray Conf (ICRC 2009), arXiv:0906.2358.

[25] The Pierre Auger Collaboration, Astropart. Phys., 2008, **29**(4): 243.

[26] C. Di Giulio, for the Pierre Auger Collaboration, Proc. 31st Int. Cosmic Ray Conf. (ICRC 2009), arXiv:0906.2189.

[27] P. Billoir, C. Roucelle, J.C. Hamilton, astro-ph/0701583.

[28] M. Settimo, for the Pierre Auger Collaboration, Proc. 32nd Int. Cosmic Ray Conf., 2011, **2**: 51, arXiv:1107.4805.

[29] The Pierre Auger Collaboration, Astropart. Phys., 2009, **31**(6): 399.

[30] G. Ros *et al.*, Astopart. Phys., 2011, **35**: 140, arXiv:1104.3399.

[31] T. Pierog, R. Engel, D. Heck, Czech. J. Phys., 2006, **56**: A161.

[32] K. Shinozaki *et al.*, Astrophys. J., 2002, **571**: L117.

[33] A. Glushkov *et al.*, Phys. Rev. D, 2010, **82**: 041101: 1.

[34] J. Ellis *et al.*, Phys. Rev. D, 2006, **74**: 115003: 1.

[35] D. Hooper, A. M. Taylor, S. Sarkar, Astropart. Phys., 2011, **34**: 340.

[36] M. Kachelriess, S. Ostapchenko, R. Tomas, Publ. Astron. Soc. Aust., 2010, **27**: 482.

[37] M. Galaverni, G. Sigl, Phys. Rev. Lett., 2008, **100**: 021102.

[38] E. Gabrielli, K. Huitu, S. Roy, Phys. Rev. D, 2006, **74**: 073002.